Journal of Applied Electrochemistry (2006) 36:1–10
DOI 10.1007/s10800-005-9020-z

Numerical model for predicting the efficiency behaviour during pulsed electrochemical machining of steel in $NaNO_3$

S. VAN DAMME[1,*], G. NELISSEN[2], B. VAN DEN BOSSCHE[2] and J. DECONINCK[1]
[1]*Vrije Universiteit Brussel TW/ETEC, Pleinlaan 2, 1050, Brussels, Belgium*
[2]*Elsyca N.V., Kraenenberg 6, 1731, Zellik, Belgium*
*(*author for correspondence, e-mail: stvdamme@vub.ac.be)*

Received 16 October 2004; accepted in revised form 4 May 2005

Key words: concentration, conductivity, efficiency, electrochemical machining, numerical model, steel, super-saturated layer, water depletion

Abstract

A new two-dimensional model is presented that allows describing the high speed electrochemical machining of steel in $NaNO_3$ solutions. Unlike existing models, local ion concentrations are calculated and used to evaluate local diffusion coefficients and electrolyte conductivity. Secondly, the presence of a super-saturated, honey-like layer on the anode surface is accounted for by introducing a water depletion factor. This factor describes the suppression of the oxygen evolution as the vast increase in ion concentrations reduces the amount of free water molecules at the anode. It is demonstrated that this approach enables to reproduce experimental average efficiency curves over a broad range of electrolyte concentrations with just a limited set of adjustable parameters.

1. Introduction

High speed electrochemical machining (ECM) is a manufacturing process based on the controlled anodic dissolution of a metal at large current densities (in the range of 1 A mm^{-2}). In ECM drilling and imaging applications, an electrolytic cell is created in which the tool (cathode) is advanced towards the work-piece (anode). The electrolyte is pumped through the electrode gap at high speed to carry away the produced heat, the dissolved metal ions and other reaction products.

When it comes to the machining of components of complex geometry and hard material, ECM has some obvious advantages over conventional milling or turning procedures: it can be applied regardless of material hardness, there is (almost) no tool wear and no thermally influenced machining zones, and a high quality surface can be obtained with no residual stresses or damage to the microstructure [1, 2]. Accordingly, many high quality parts are prepared with ECM, from shaver heads to turbine blades.

Despite its advantages some difficulties still trouble the application of ECM. One important issue is the lack of advanced quantitative simulation software to predict the tool shape and machining parameters necessary to produce a given work-piece profile [3, 4]. The prevailing conditions during ECM complicate a numerical simulation in several ways. A complete model needs to deal with the effects of fluid flow, gas evolution and heat generation, with the electrochemical processes at both electrodes and with the transport of the species involved. Even when not all effects are taken into account, the strong variations in physical quantities require a refined mesh, particularly near the electrodes, while the large deviations from dilute solution theory call for an adapted physical model. This prolongs computations and hinders a smooth and fast convergence. Therefore, a compromise has to be found between the feasibility and the accuracy of the simulation, certainly when pulsed ECM is considered and time accurate simulations are required.

Most existing models for ECM assume constant electrolyte conductivity [4–7]. In more refined models the influence of the temperature and the gas fraction on the electrolyte conductivity is accounted for [8, 9]. Probably more important than the gas fraction is the influence of the ion concentrations. Mount et al. have found that the negative influence of the gas fraction on the electrolyte conductivity can be outweighed by the increase in ion concentrations and resistive heating [4]. A reliable estimation of the local electrolyte conductivity is important as it is inextricably tied to the current density distribution and thus to the final shape of the work-piece.

Aside from the electrolyte conductivity, another quantity determines the performance of an ECM

process: the current efficiency. In the case of electrochemical machining of steel in $NaNO_3$, oxygen gas evolution proceeds in parallel with metal dissolution, their ratio depending notably on the overpotential and the free water activity. The latter falls dramatically with the formation of a super-saturated layer on the anode [3]. As metal is continuously discharged from the anode, the adjacent solution becomes saturated and eventually transforms into a meta-stable liquid consisting of iron nitrates. The small number of water molecules still present in this layer will be bound to the ions, thus restricting the source of oxygen evolution [3]. Consequently, more current will be absorbed for metal dissolution, thus increasing the current-efficiency and reinforcing the saturation.

In this paper a new two-dimensional model for ECM is presented. Though not mathematically rigorous, the model captures the important effects of high ion concentrations on the physical properties of the electrolyte and allows to estimate the current efficiency in a fast way. It focuses on the electrochemical machining of steel work-pieces in $NaNO_3$ solutions. The model is validated by comparing simulated average efficiency curves with experimentally obtained curves.

2. Mathematical model

The flow in the electrode gap is in principle a two-phase flow as gas evolution occurs at both the cathode and the anode. However, the gas fraction is deliberately suppressed in many industrial applications by working at elevated pressure and high flow rates. If no gas evolution is considered, the flow is governed by the incompressible Navier-Stokes equations, expressing the conservation of mass and momentum. Because the flow in the electrode gap is turbulent at high flow rates, the Reynolds Averaged Navier-Stokes (RANS) model is used in this work. The turbulent viscosity, which enters these equations, is calculated with the low-Re k-ω turbulence model. A detailed description of the equations, the boundary conditions and the numerical solution techniques can be found in references [10, 11]. The amount of metal removed during one ECM pulse is negligible, such that the electrode shape remains unaltered and the flow may be regarded as stationary.

In this paper, the fluid and the electrodes are considered isothermal, which is a valid assumption during the first ECM pulses because the amount of energy inserted during one ECM pulse is quite low. Thermal effects will manifest themselves only on a longer timescale. An extension of the mathematical model and solver to treat non-isothermal problems will be presented in future work.

In the following paragraphs the computation of the potential distribution and the transport of the electrolyte species will be discussed.

2.1. *The potential distribution in the electrolyte*

When considering the ECM process at high flow rates, very thin concentration boundary layers are formed at the electrodes. Outside these boundary layers the composition is uniform such that the potential satisfies Laplace's equation. Inside the concentration boundary layers, however, concentrations will rise sharply and change the electrolyte conductivity significantly. Hence, instead of using Laplace's equation for the potential distribution, a more elaborate expression is adopted in this paper:

$$\overrightarrow{\nabla} \cdot (\kappa \overrightarrow{\nabla} U) = 0. \tag{1}$$

with U the solution potential (V), and κ the local electrolyte conductivity (S m^{-1}). κ is calculated as for infinitely diluted solutions:

$$\kappa = \frac{F^2}{RT} \sum_i z_i^2 D_i c_i. \tag{2}$$

with z_i the valency, D_i the diffusion coefficient (m^2 s^{-1}), c_i the concentration (mol m^{-3}), F the Faraday constant, R the universal gas constant, and T the temperature (K).

The boundary conditions related to the potential distribution are [10]:

- at insulators and symmetry planes:

$$\frac{\partial U}{\partial n} = 0, \tag{3}$$

- at inlets and outlets:

$$\overrightarrow{\nabla} U = 0, \tag{4}$$

- at electrodes:

$$J_k = f(V - U, c_{i \in k}) \tag{5}$$

with J_k the reaction current density (A m^{-2}), V the electrode potential (V), U the potential at the solution side of the double layer, and $c_{i \in k}$ the concentrations of the ions participating in the reaction (mol m^{-3}).

On the cathode the reduction of water produces hydrogen gas and hydroxide ions [12]:

$$2H_2O + 2e^- \rightarrow H_2 + 2OH^-. \tag{6}$$

On the anode two types of reactions occur simultaneously. On the one hand steel dissolves into metal ions (mainly Fe^{2+}, Fe^{3+} and Cr^{6+}), considered here as a single species with valency z:

$$Me \rightarrow Me^{z+} + z\,e^-, \tag{7}$$

while on the other hand water is oxidized to oxygen gas [3]:

$$2H_2O \rightarrow O_2 + 4H^+ + 4e^-. \tag{8}$$

The polarization behaviour is linearized for all electrode reactions:

$$J_k = \frac{V - U - Q_k}{R_k}. \tag{9}$$

with R_k the polarization resistance and Q_k the onset of polarization, i.e. the minimum required $V-U$ to initiate the reaction. This approximation is justifiable for the considered ECM process, because Altena et al. found a linear dependence of the total activation overpotential on the current density [12]. More accurate (non-linear) polarization behaviour, e.g. Butler-Volmer kinetics, will be investigated and presented in future papers.

2.2. *Transport equations*

The conservation of mass for each species in a solution in which the flow is determined by the solvent and in the absence of homogenous reactions, implies that the change of concentration in an infinitesimally small control volume is equal to the net input [13]:

$$\frac{\partial c_i}{\partial t} = -\vec{\nabla}\,\vec{N_i} \tag{10}$$

with $\vec{N_i}$ the flux (mol m^{-2} s^{-1}). To reduce the amount of unknowns the above equation is implemented only for the active ions, i.e. Me^{z+} and OH^-. It is assumed that NO_3^- and Na^+ of the supporting electrolyte neutralize the excess charges of both ions respectively:

$$c_{Na^+} = c_{Na^+,\mathrm{bulk}} + c_{OH^-}, \tag{11}$$

$$c_{NO_3^-} = c_{NO_3^-,\mathrm{bulk}} + z\,c_{Me^{z+}}. \tag{12}$$

The fluxes are calculated as follows:

$$\vec{N_i} = c_i\vec{v} - D_i\vec{\nabla}c_i. \tag{13}$$

with $\vec{v}$ the fluid velocity (m s^{-1}). The first term corresponds to convection and the second term to molecular diffusion. As a first approximation, the migration term is disregarded to reduce coupling between the equations via the potential. In future work, this shortcoming will further be dealt with. By using these flux equations the mass conservation equations reduce to convective diffusion equations:

$$\frac{\partial c_i}{\partial t} + \vec{v}.\vec{\nabla}c_i = \vec{\nabla}.(D_i\vec{\nabla}c_i). \tag{14}$$

The boundary conditions are [10]:

- at insulators and symmetry planes:

$$\frac{\partial c_i}{\partial n} = 0, \tag{15}$$

- at inlets:

$$c_i = c_{i,\mathrm{bulk}}, \tag{16}$$

- at outlets:

$$\vec{\nabla}c_i = 0, \tag{17}$$

- at electrodes, for the active species (involved in only one electrode reaction):

$$\frac{\partial c_i}{\partial n} = \frac{j_i}{z_i F D_i}. \tag{18}$$

Equations 5 and 18 form the coupling between the potential distribution and the concentration distributions.

2.3. *Specific equations for the ECM process*

At the anode, the massively produced metal ions displace and coordinate the water molecules, until almost no free water molecules are present [3]. Consequently, the rate of oxygen evolution is reduced. To capture this effect, the right hand side of equation 9 for the oxygen evolution is multiplied with a water depletion factor w. Because the water concentration is not explicitly calculated, the factor is based on the metal ion concentration:

$$w = \frac{1}{2}\left[1 + \cos\left(\pi\frac{c_{Me^{z+}} - c_{Me^{z+}}^{\mathrm{begin}}}{c_{Me^{z+}}^{\mathrm{end}} - c_{Me^{z+}}^{\mathrm{begin}}}\right)\right]. \tag{19}$$

This function has been chosen to ensure a smooth transition between no depletion (up to $c_{Me^{z+}}^{\mathrm{begin}}$) and total depletion (from $c_{Me^{z+}}^{\mathrm{end}}$ on), but can be replaced by an empirical function in future work.

To respond to the strengthening of ion-ion interactions in the highly concentrated boundary layers the diffusion coefficients in Equations 2 and 14 are made concentration dependent. Reasonable expressions are derived from the work of Lohrengel et al. [3]. The expressions are modified in two ways: (1) the ionic strength is chosen as a measure of the sum of all ion concentrations instead of the nitrate concentration, and (2) a minimum diffusion coefficient is added to describe the lowered but non-zero transport rate of ions through the super-saturated layer. This leads to the following type of function:

$$D_i = D_{0,i}\exp\left(-\frac{a_i}{z_i^2}I\right) + D_{\min,i} \tag{20}$$

with I the ionic strength (mol m^{-3}), $D_{0,i}$ the diffusion coefficient at infinite dilution (m^2 s^{-1}), $D_{min,i}$ the diffusion coefficient at infinite ionic strength (m^2 s^{-1}), and a_i a fitting parameter (m^3 mol^{-1}). The concentration of Me^{z+} is artificially limited to 5 mol l^{-1} in the calculation of the ionic strength and the conductivity. This value is estimated from the density of the super-saturated layer (around 1500 g l^{-1} [3]) and the molecular weights of $Fe(NO_3)_3.9H_2O$ (MW = 404 g mol^{-1}) and $Fe(NO_3)_2.6H_2O$ (MW = 288 g mol^{-1}). Limiting the concentration of Me^{z+} prevents the conductivity to rise again at very high concentrations when the diffusion coefficients have reached their minimum value.

2.4. *Summary*

The electrochemistry of the model involves three unknowns, i.e. U, $c_{Me^{z+}}$ and c_{OH^-}, satisfying three Equations: 1, 14 (for Me^{z+}) and 14 (for OH^-). In fact, the Equations 14 serve two purposes: (1) to correct the

local electrolyte conductivity for changes in the ion concentrations according to Equation 2, and (2) to introduce a water depletion factor defined by Equation 19. All diffusion coefficients in Equations 2 and 14 depend on the local ionic strength as expressed by Equation 20.

2.5. *Numerical aspects*

All partial differential equations presented above are discretized in two dimensions with a triangular mesh, using the Finite Element method with upwind contributions for the convection terms [14]. The scalar N-scheme is applied to the convective terms in Equation 14. All the numerical schemes provide at least second order accuracy [11]. The resulting non-linear systems of equations are linearized with the Newton-Raphson method. A second order implicit time accurate time integration scheme is used to treat the time dependent terms in Equation 14 [15].

At each time step solving Equation 1 with boundary conditions 3–5 provides the potential distribution and the partial current densities along the electrodes. The partial current densities are linked to the local ion fluxes at the electrodes through Equations 18, so that the mass transfer Equations 14 for Me^{z+} and OH^- can be solved. These concentrations influence the local conductivity so that some Newton iterations are needed until converged potential and concentration fields are obtained and the next time step can be computed.

3. Results and discussion

In order to validate the numerical ECM model, simulated results have been compared with experimental results. Altena et al. [12] measured average efficiency curves in a parallel plate flow channel with dimensions shown in Figure 1. A sufficiently long entrance zone was foreseen to attain a fully developed flow profile. The electrolyte was forced through the channel at a speed of approximately 15 m s^{-1}, assuring a fully turbulent flow (Re = 8200). All simulations have been performed for the same reactor configuration and flow conditions. In principle, the turbulent diffusivity needs to be considered for the ion conservation equations. However, many turbulent diffusivity models exist and give widely differing values [14]. Because the electrode length is not too far above the criterium of short electrodes, the turbulent diffusivity is neglected.

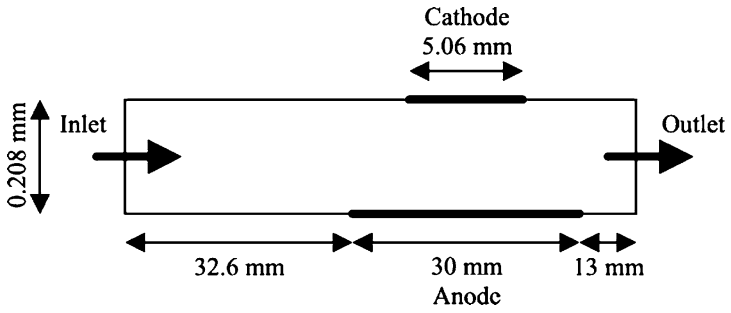

Fig. 1. Schematic representation of the reactor geometry.

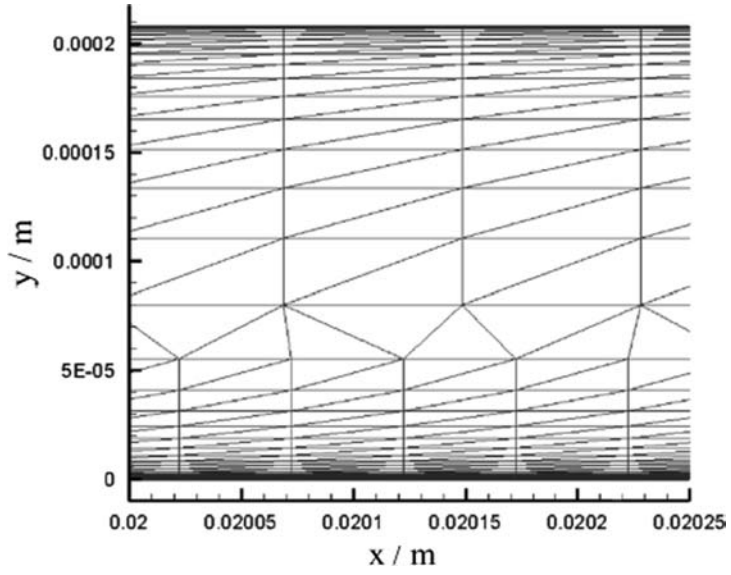

Fig. 2. Zoom of the grid in the flow channel.

A zoom of the grid in the flow channel is shown in Figure 2. In order to capture properly the hydrodynamic and concentration boundary layers, aligned and very stretched elements (aspect ratio of 1000 for the first element) have been used. The first grid points are placed at a distance of 50 nm from the electrode.

Rectangular pulsed currents with a total period of 100 ms and with on-times of 1, 2, 5 and 10 ms have been applied. Preliminary simulations have proven that the off-times (≥90 ms) suffice to reestablish the bulk concentrations. Hence, the current pulses can be regarded as independent. This simplifies considerably the calculations and the interpretation of the measurements.

To compare with the experiments, the simulated local current efficiencies have been averaged over the anode's surface and over the elapsed time. The average efficiency is then obtained as a function of the average current density on the cathode for different pulse durations.

The average efficiency measured on stainless steel ASN-N004 (85.28% Fe, 14% Cr) in reference [12] tends to a maximum level around 83% at large current density and pulse duration for various concentrations of $NaNO_3$. The average efficiency was defined on dissolution into Fe^{2+} and Cr^{6+}, corresponding to an average valency of about 2.5. If this maximum level signifies that all the current is consumed for metal dissolution, than the true average valency will be 3, indicating dissolution into other species as well, e.g. Fe^{3+}. Mount et al. measured average valencies for various stainless steels [16]. They found a value of 3.5 for the comparable stainless steel SS410 (85.50% Fe, 12.75% Cr). In this work, an average metal ion valency of 3 is chosen.

3.1. *Identifying and quantifying the model parameters*

The diffusion parameters $D_{0,i}$ and a_i are taken from reference [3] and are listed in Table 1. $D_{0,Me^{z+}}$ is considered equal to $D_{0,Fe^{3+}}$, D_{0,OH^-} is taken from reference [13] and a_{OH^-} is assigned the same value as $a_{NO_3^-}$. Each ion is given the same $D_{\min,i}$, because no exact values were found, nor was there any indication that it would significantly improve the model. When comparing the case of the $D_{\min,i}$ having values such that their ratio's are the same as for the $D_{0,i}$ to the case of every $D_{\min,i}$ having the same average value, the current efficiency never changes by more than 0.1%.

The polarization parameters R_k and Q_k of the electrode reactions are listed in Table 2. The polarization parameters R_{H_2} and Q_{H_2} of the hydrogen evolution are derived from the Tafel coefficients on iron [17]. No separate information regarding the anodic reactions was found in literature, because iron dissolution is always accompanied by oxygen evolution. A combined polarization resistance R_a and onset of polarization Q_a is obtained by subtracting the contribution of the hydrogen evolution from the total overpotential measured by Altena et al. [12].

Table 1. Diffusion parameters of the ions [3]

	z_i	$10^9 D_{0,i}/m^2\ s^{-1}$	$10^{\ 3} a_i/\ m^3\ mol^{-1}$
Me^z+	+3	1.24	1.14
OH^-	−1	5.18	0.238
Na^+	+1	1.33	0.33
NO_3^-	−1	1.90	0.238

Table 2. Polarization parameters

R_{H_2}	0.1 Ω mm^2
Q_{H_2}	−1 V
R_a	3.0 Ω mm^2
Q_a	2.3 V

The remaining model parameters are: (1) the minimum diffusion constant D_{min} (the same for each ion), (2) the concentration interval in which water depletion sets in $[c^{begin}_{Me^{z+}}, c^{end}_{Me^{z+}}]$, (3) the shift in onset of polarization between the metal dissolution and the oxygen evolution $q = Q_{Me^{z+}} - Q_{O_2}$ and (4) the ratio of the polarization resistances of the metal dissolution and the oxygen evolution $r = \frac{R_{Me^{z+}}}{R_{O_2}}$. These four parameters have been adjusted to obtain optimal agreement between simulation and experiment for a 250 g $NaNO_3$ l^{-1} solution. The results are shown in Figure 3 and the corresponding values are listed in Table 3. The value of 10^{-11} m^2 s^{-1} for D_{min} is comparable to diffusion coefficients of water in paint and polymer films [18]. At an intermediate concentration of 130 g $NaNO_3$ l^{-1} (not shown) and even at a much lower concentration of 70 g $NaNO_3$ l^{-1} (shown in Figure 4) the same set of values accurately predicts the average efficiency.

The root mean square deviations between the simulated and the experimental average efficiency in the interval between 0.3 and 1.1 A mm^{-2} are listed in Table 4. They are roughly equal to 6%. The highest deviations are found at the longest pulses. The main reason for this is that the instantaneous efficiency temporarily exceeds the maximum level [12], which may signify a lowering of metal valency during the pulse. Writing individual metal dissolution reactions would solve this problem, however quantitative data are still lacking [3].

Nevertheless, the simulated average efficiency clearly exhibits the same behaviour as experimentally observed: no influence of the pulse duration at small current density, a steep gradient at intermediate current density and a leveling off at large current density. The transitions between these characteristic regions are shifted to larger current densities for shorter pulses and lower $NaNO_3$ concentrations. In references [19, 20] the breakdown of metal passivity was considered to determine the efficiency behaviour of nickel in $NaNO_3$ solutions. In this work, an alternative explanation is proposed based on the presence of the super-saturated layer. At small current density and pulse duration no sufficient concentration of iron ions can be built up at the anode to cause water depletion. Consequently the average efficiency is fixed. This situation is more persistent at low $NaNO_3$ concentrations, because the local diffusion coefficients

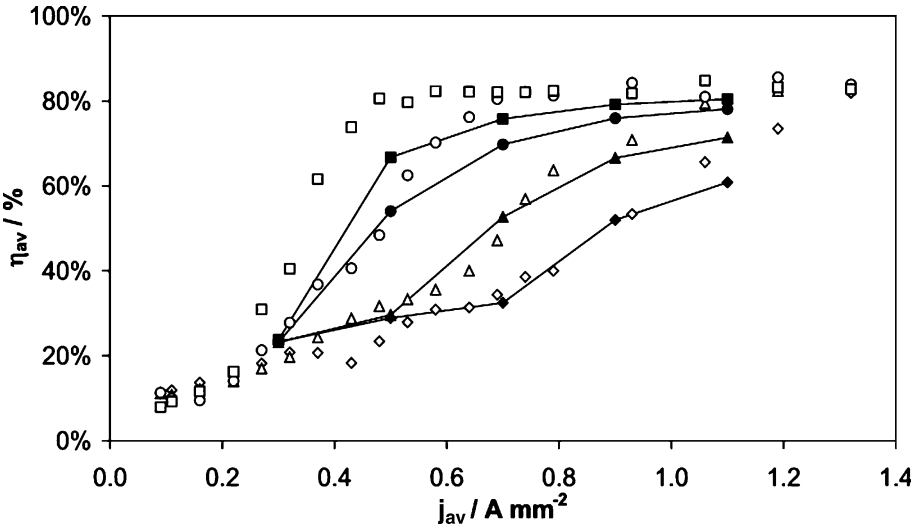

Fig. 3. Comparison of experimental and simulated average efficiency curves for different pulse durations t_p at 250 g $NaNO_3$ l^{-1}. Experimental curves: $t_p = 1$ ms (◇), $t_p = 2$ ms (Δ), $t_p = 5$ ms (○), $t_p = 10$ ms (□). Simulated curves: $t_p = 1$ ms (♦), $t_p = 2$ ms (▲), $t_p = 5$ ms (●), $t_p = 10$ ms (■).

are higher. At a certain current density and pulse duration the onset of water depletion causes the efficiency to rise. This rise is quite abrupt because the process of water depletion is self-reinforcing. Figure 5 illustrates this sudden change by showing the partial current densities of iron dissolution and oxygen evolution along the anode at 0.8 ms, 1.5 ms and 5 ms for an average current density of 0.7 A mm^{-2}. After 0.8 ms there is still uniform accessibility for water to the anode. After 1.5 ms the metal ion concentration is already so high that water can reach the anode only at its edges. The upstream edge is still accessible after 5 ms, because the lateral expansion of the super-saturated layer by diffusion is counteracted by convection. The downstream edge has clearly become less accessible for water, because diffusion and convection cooperate to expand the super-saturated layer.

Finally the average efficiency tends to a limiting value independent of current density, pulse duration and

Table 3. Optimized values of the adjustable model parameters at 250 g $NaNO_3$ l^{-1}

D_{min}	10^{-11} m^2 s^{-1}
$[c^{begin}_{Me^{z+}}, c^{end}_{Me^{z+}}]$	[0.5 mol l^{-1}, 1.75 mol l^{-1}]
r	1.3
q	0.6 V

Table 4. RMS deviations between the simulated and the experimental average efficiency curves for different concentrations and pulse durations

c_{NaNO_3}/ g l^{-1}	t_p = 1 ms	t_p = 2 ms	t_p = 5 ms	t_p = 10 ms
70	4.54%	7.58%	6.03%	5.56%
130	4.25%	5.03%	6.03%	6.75%
250	3.71%	4.36%	7.33%	11.40%

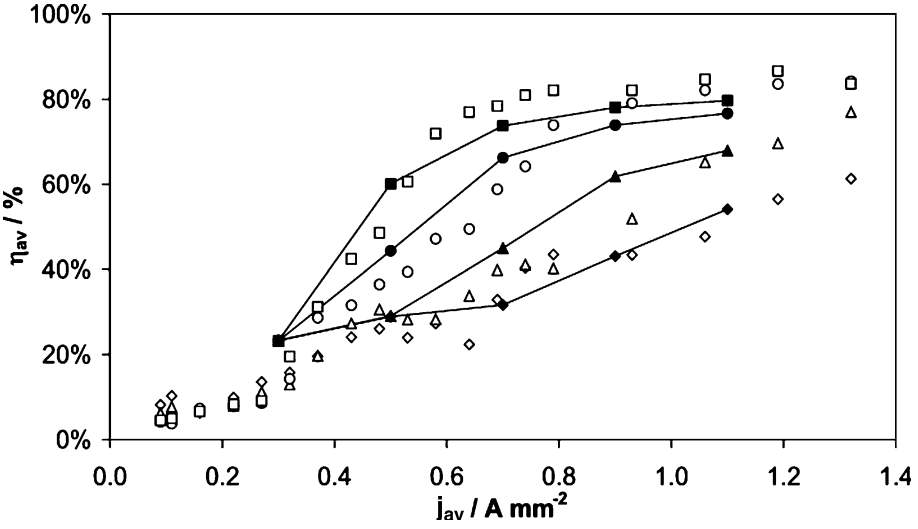

Fig. 4. Comparison of experimental and simulated average efficiency curves for different pulse durations t_p at 70 g $NaNO_3$ l^{-1}. Experimental curves: $t_p = 1$ ms (◇), $t_p = 2$ ms (Δ), $t_p = 5$ ms (○), $t_p = 10$ ms (□). Simulated curves: $t_p = 1$ ms (♦), $t_p = 2$ ms (▲), $t_p = 5$ ms (●), $t_p = 10$ ms (■).

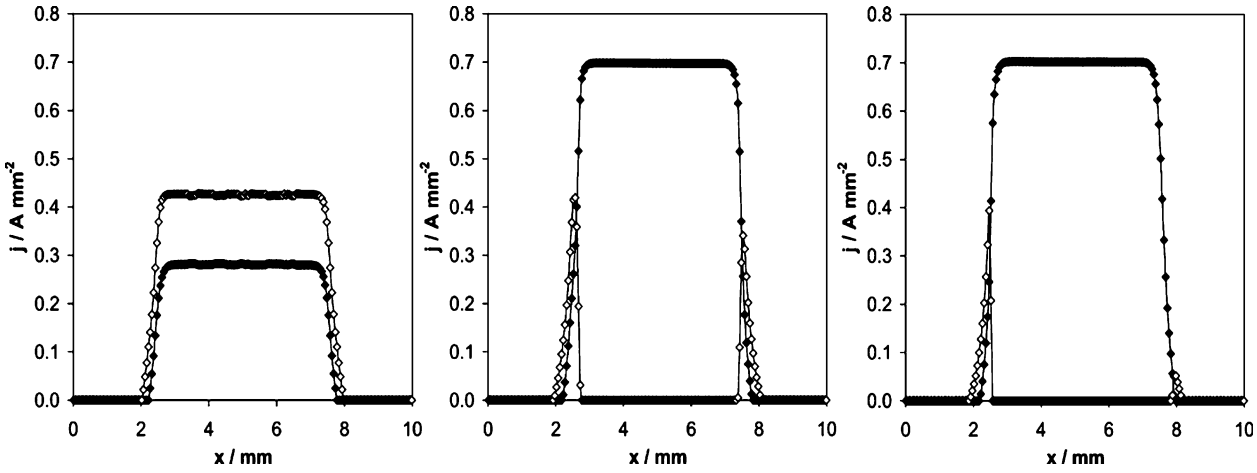

Fig. 5. Partial current densities of iron dissolution $j_{Fe}2.5+$ (♦) and oxygen evolution j_{OH-} (◇) on the anode at 0.8 ms (left), 1.5 ms (center) and 5 ms (right). The average current density is 0.7 A mm^{-2}.

concentration, because metal dissolution is the sole reaction.

3.2. *Sensitivity of the simulations to the model parameters*

For a solution of 250 g $NaNO_3$ l^{-1} a sensitivity study has been performed to examine the role of the four adjustable model parameters on the simulations. The average efficiency is calculated in the three characteristic regions for a higher and a lower value of each parameter.

First the minimum diffusion constant D_{min} is in turn increased and decreased by an order of magnitude. Figure 6 shows the impact on the simulated average efficiency curves. No change occurs at the small current density and pulse duration. At larger current density a decrease by an order of magnitude results in lower average efficiencies, particularly for short pulses. Care has to be exercised when choosing high values, because it may adversely affect the behaviour of the electrolyte conductivity. The minimum diffusion constant must be chosen low enough so that the minimum in the conductivity curve would occur after the concentration of Me^{z+} has reached its saturation at 5 mol l^{-1}.

Figure 7 shows the effect of shifting the concentration interval $[c^{begin}_{Me^{z+}}, c^{end}_{Me^{z+}}]$ in which water depletion sets in. A shift of 0.25 mol l^{-1} to higher and lower concentrations respectively leads to a decrease and an increase in the average efficiency. Again the effect is stronger for large current densities and short pulses. These observations agree with the fact that if current density and pulse duration are kept small enough, mass transport will be sufficient to avoid water depletion. Hence, the discussed parameters will not influence the efficiency. At larger current density water depletion sets in at a given

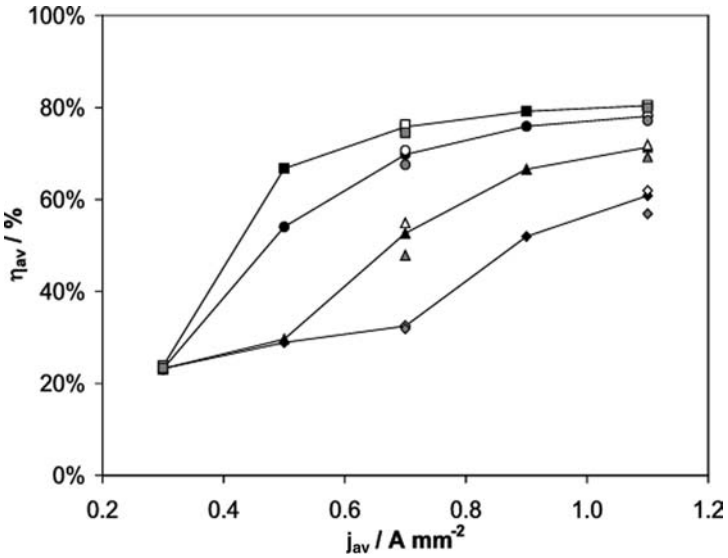

Fig. 6. Influence of the minimum diffusion constant on the simulated average efficiency curves: $D_{min} = 10^{-12}$ m^2 s^{-1} (white symbols), $D_{min} = 10^{-10}$ m^2 s^{-1} (grey symbols). Simulated curves at $D_{min} = 10^{-11}$ m^2 s^{-1}: $t_p = 1$ ms (♦), $t_p = 2$ ms (▲), $t_p = 5$ ms (●), $t_p = 10$ ms (■).

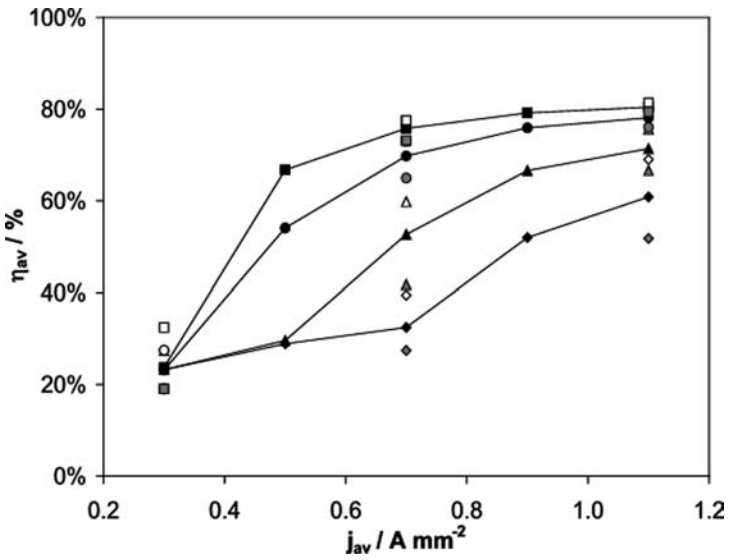

Fig. 7. Influence of the concentration interval in which water depletion sets in on the simulated average efficiency curves: [c^{begin}, c^{end}] = [0.25 mol l^{-1}, 1.50 mol l^{-1}] (white symbols), [c^{begin}, c^{end}] = [0.75 mol l^{-1}, 2.00 mol l^{-1}] (grey symbols). Simulated curves at [c^{begin}, c^{end}] = [0.50 mol l^{-1}, 1.75 mol l^{-1}]: t_p = 1 ms (♦), t_p = 2 ms (▲), t_p = 5 ms (●), t_p = 10 ms (■).

moment and the instantaneous efficiency will rapidly increase due to the self-reinforcing mechanism, until it reaches a maximum. The chosen concentration interval naturally affects the onset of water depletion. The minimum diffusion constant is involved indirectly for it determines the removal rate of the ions. Because the simulated efficiency is averaged over the elapsed time, it will initially increase fast and then gradually level off to the maximum, explaining the enhanced sensitivity to both parameters for short pulses.

The two other model parameters describe the polarization behaviour of the anodic reactions. In Figure 8 it is shown that a larger shift in onset of polarization leads to an overall decrease in the average efficiency and vice versa. A similar observation is made in Figure 9 for the ratio of the polarization resistances. The shift in onset of polarization influences the average efficiency more at small current density, while the influence of the ratio of the polarization resistances shows no clear dependence on current density. A strong influence is noticed in both cases near the point where the slope of a curve suddenly increases.

In order to explain these observations, it is interesting to consider the hypothetical case of no water depletion. Then the average efficiency will have a fixed value at each average current density, determined by the polarization behaviour of the anodic reactions. For uniform electrolyte conductivity and without edge effects, the

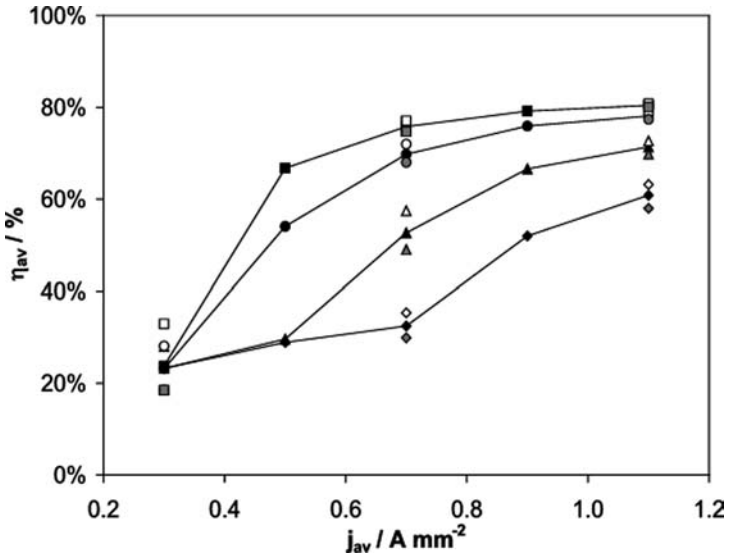

Fig. 8. Influence of the shift in onset of polarization between the iron dissolution and the oxygen evolution on the simulated average efficiency curves: q = 0.5 V (white symbols), q = 0.7 V (grey symbols). Simulated curves at q = 0.6 V: t_p = 1 ms (♦), t_p = 2 ms (▲), t_p = 5 ms (●), t_p = 10 ms (■).

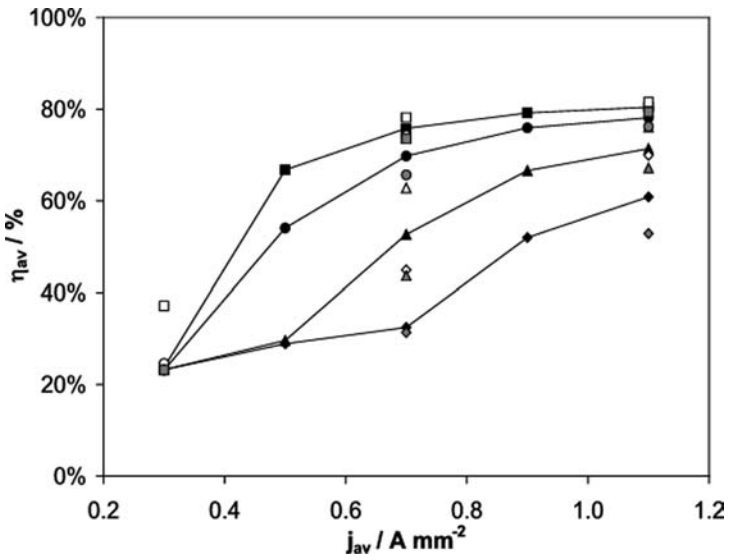

Fig. 9. Influence of the ratio of the polarization resistances on the simulated average efficiency curves: $r = 1.0$ (white symbols), $r = 1.6$ (grey symbols). Simulated curves at $r = 1.3$: $t_p = 1$ ms (♦), $t_p = 2$ ms (▲), $t_p = 5$ ms (●), $t_p = 10$ ms (■).

average efficiency can be derived directly from the applied current density, according to:

$$\eta_{av} = \frac{1}{1+r} - \frac{rq}{(1+r)^2 R_a}\frac{1}{j} \tag{21}$$

with η_{av} the average efficiency and j the total current density (A m^{-2}). The second term is dominant at low current density and is influenced by both parameters q and r, while the first term is dominant at high current density and is influenced only by r. This behaviour corresponds with the observed dependences in Figures 8 and 9. The strong dependence where the slope of a curve suddenly increases, is explained by the fact that in this region water depletion sets in. The onset is influenced indirectly by the polarization behaviour of the electrode reactions, i.e. by q and r, because it determines the supply of metal ions.

It can be concluded that the polarization behaviour of the electrode reactions determines a basic average efficiency curve. Once water depletion sets in the average efficiency departs from this curve, increasing fast before gradually leveling off to a maximum. This point of departure is influenced by all model parameters.

4. Conclusions

A model for ECM in $NaNO_3$ solutions that accounts for the effects of local concentration variations has been developed. Diffusion coefficients and electrolyte conductivity have been made concentration dependent. A factor describing the suppression of oxygen evolution as a result of water depletion has been defined. The model has been implemented for two-dimensional reactor configurations. Literature data have been used to determine the model parameters. Excellent agreement between experimental and simulated curves is achieved for different electrolyte concentrations, with the same parameters.

A sensitivity study has revealed that the average efficiency curves may be considered as a superposition of two curves. At small current densities and for short pulses the average efficiency is time independent and solely determined by the polarization behaviour of the electrode reactions. In this region water is still abundant at the anode. At larger current densities and for longer pulses a steep gradient marks the onset of water depletion. This turning point is subject to all model parameters. Finally the average efficiency tends to a maximum value.

Acknowledgement

The financial support of the European Commission (Growth G1RD-CT2000-00421 SPECTRUM) is gratefully acknowledged.

References

1. D.G. Risco and A.D. Davydov, *J. Am. Soc. Mech. Eng.* **64** (1993) 701.
2. J.A. McGeough, *Principles of Electrochemical Machining* (Chapman and Hall, London, 1974).
3. M.M. Lohrengel, I. Klüppel, C. Rosenkranz, H. Betterman and J.W. Schultze, *Electrochim. Acta* **48** (2003) 3203.
4. A.R. Mount, D. Clifton, P. Howarth and A. Sherlock, *J. Mater. Proc. Technol.* **138** (2003) 449.
5. D. Zhu and H.Y. Xu, *J. Mater. Proc. Technol.* **129** (2002) 15.
6. P. Domamowski and J. Kozak, *J. Mater. Proc. Technol.* **109** (2001) 347.
7. S. Das and A.K. Mitra, *Int. J. Numer. Methods Eng.* **35** (1992) 1045.
8. C.S. Chang and L.W. Hourng, *J. Appl. Electrochem.* **31** (2001) 145.

9. S. Bhattacharyya, A. Ghosh and A.K. Mallik, *J. Mater. Proc. Technol.* **66** (1997) 146.
10. G. Nelissen, B. Van den Bossche, J. Deconinck, A. Van Theemsche and C. Dan, *J. Appl. Electrochem.* **33** (2003) 863.
11. N. Waterson, Simulation of Turbulent Flow, Heat and Mass Transfer Using a Residual-Distribution Approach, Dissertation (Technische Universiteit Delft, 2003).
12. H.S.J. Altena, Precision ECM by Process Characteristic Modelling, Dissertation (Glasgow Caledonian University, 2000). A.K.M. De Silva, H.S.J. Altena and J.A. McGeough, *Ann. CIRP*, **49** (2000) 151.
13. J.S. Newman (Ed.), Electrochemical Systems, 2nd edn. (Prentice-Hall, Englewood Cliffs, NJ, 1991).
14. G. Nelissen, A. Van Theemsche, C. Dan, B. Van den Bossche and J. Deconinck, *J. Electroanal. Chem.* **563** (2004) 213.
15. C. Dan, B. Van den Bossche, L. Bortels, G. Nelissen and J. Deconinck, *J. Electroanal. Chem.* **505** (2001) 12.
16. A.R. Mount, P.S. Howarth and D. Clifton, *J. Electrochem. Soc.* **150** (2003) D63.
17. D.J. Pickett, *Electrochemical Reactor Design* (Elsevier, Amsterdam, 1977).
18. E.L.J. Goossens, A.J.J. van der Zanden, H.L.M Wijen and W.H. van der Spoel, *Prog. Org. Coat.* **48** (2003) 112.
19. M. Datta, H.J. Mathieu and D. Landolt, *Electrochim. Acta* **24** (1979) 843.
20. M. Datta and D. Landolt, *J. Electrochem. Soc.* **124** (1977) 483.